

SOLUTION AND SOLID-STATE AGGREGATION PROPERTIES OF 4-MERCAPTOPYRIDINE-4-THIOPYRIDONE

MARGARET C. ETTER,* JOHN C. MACDONALD AND RANDALL A. WANKE

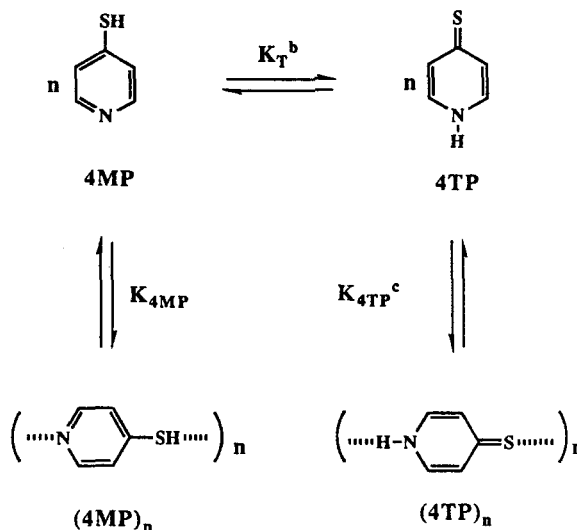
Department of Chemistry, University of Minnesota, Minneapolis, Minnesota 55455, USA

The hydrogen-bond pattern of 4-mercaptopyridine-4-thiopyridone in solution and in the solid state consists of extended chains of 4-thiopyridone associated through $\text{NH}\cdots\text{S}$ hydrogen bonds. The solution structure in chloroform was studied by UV–visible spectrometry and vapor pressure osmometry. A tautomerization constant of 1.8, favoring 4-thiopyridone, and a self-association constant of 2600 mf^{-1} were determined. Over 50% of the sample is aggregated near saturation with significant amounts (>15%) of the sample present as oligomers containing four or more 4-thiopyridone monomer units. In its crystal structure, 4-mercaptopyridine-4-thiopyridone is composed of infinite chains of 4-thiopyridone associated by $\text{NH}\cdots\text{S}$ hydrogen bonds between glide related molecules, with $\text{N}\cdots\text{S} = 3.219(3) \text{ \AA}$, $\text{H}\cdots\text{S} = 2.42(4) \text{ \AA}$, $\text{N}-\text{H}\cdots\text{S}$ angle = $175(4)^\circ$ and $\text{H}\cdots\text{S}=\text{C}$ angle = $96(1)^\circ$. Relationships between solution aggregation, crystal nucleation, and crystal propagation are discussed. Crystal data are as follows: space group = $P2_1/c$, $a = 7.183(5) \text{ \AA}$, $b = 6.132(5) \text{ \AA}$, $c = 11.618(7) \text{ \AA}$, $\beta = 90.51(5)^\circ$, $Z = 4$, $D_c = 1.44 \text{ g cm}^{-3}$, 1623 reflections, $R = 0.050$, $R_w = 0.072$.

INTRODUCTION

A question that has intrigued us for some time is whether hydrogen-bonded aggregates found in crystal structures have their origin as solution aggregates, perhaps even serving as nucleation sites for crystallization, or whether they form by addition of a single molecule at a time to a growing crystal surface. Analyses of large numbers of crystal structures of hydrogen-bonded compounds have suggested that solution aggregation drives crystallization,¹ but to date we have not investigated the solution properties of these compounds in detail.

We report here the structure and concentration of hydrogen-bonded aggregates of 4-mercaptopyridine-4-thiopyridone (**I**) in chloroform solution, and the crystal structure of **I**. As shown in Scheme 1, 4-mercaptopyridine (4MP) and 4-thiopyridone (4TP) are in equilibrium in solution with their multiply hydrogen-bonded oligomeric species, $(4\text{MP})_n$ and $(4\text{TP})_n$. A similar situation occurs for the oxo analog, 4-hydroxypyridine-4-pyridone (**II**), which has been studied before but primarily in solution.² The dominant tautomeric form of **I** in chloroform solution is 4TP. Values for the tautomerization constant (K_T) and self-association constant ($K_{4\text{TP}}$) are determined from



Scheme 1. The analogous descriptors for the 4-hydroxypyridine-4-pyridone system are 4P, $(4\text{P})_n$, 4HP and $(4\text{HP})_n$.^b The tautomerization constant $K_T = X_{4\text{TP}}/X_{4\text{MP}}$.^c The self-association is for the stepwise formation of hydrogen-bonded oligomer, e.g. $K_{4\text{TP}} = X_{(4\text{TP})_n}/X_{(4\text{TP})_{n-1}}X_{4\text{TP}}$

* Alfred P. Sloan Fellow, 1989–91. Author for correspondence.

UV-visible spectrometry and vapor pressure osmometry measurements. At saturation, over 50% of **I** in chloroform is aggregated into dimers or higher oligomers. In the crystal structure, **I** is also found to form hydrogen-bonded chains of 4TP. A discussion of the implications of these results for understanding molecular recognition and crystal growth is given.

EXPERIMENTAL

General methods. ^1H and ^{13}C NMR spectra were recorded on an IBM NR200F spectrometer (200 MHz). Chemical shifts are in ppm (δ) from TMS. Infrared spectra (Nujol) were recorded on a Nicolet 5DXB Fourier transform spectrometer. UV-visible solution spectra were recorded on a Hewlett Packard Model 8452A diode-array spectrophotometer using cells of 0.01, 0.1 and 1 cm path length. X-ray powder diffraction was performed using a Philips powder camera with Cu radiation. Vapor pressure osmometry measurements were done on a Wescan Model 2332 vapor pressure osmometer at 25°C, calibrated in chloroform using sucrose octaacetate as a non-associating standard. Melting points were recorded on a Fisher-Johns apparatus (uncorrected).

4-Mercaptopyridine-4-thiopyridine (I). Technical grade (90%) **I**, purchased from Aldrich, was recrystallized twice from hot spectroscopic-grade toluene. Slow evaporation from toluene yielded odorless, yellow hexagonal crystals ($0.50 \times 0.50 \times 0.25$ mm) for single crystal X-ray diffraction; m.p. 140–170°C, the crystals slowly turning dark yellow over the melting range and giving off a pungent odor; IR (Nujol), 3192, 2801, 2634, 1612, 1110, 795 cm^{-1} ; ^1H NMR ($\text{DMSO}-d_6$) δ 7.18–7.21 (d, 2H, $J = 5.88$), 7.59–7.62 (d, 2H, $J = 6.19$) ppm; ^{13}C NMR ($\text{DMSO}-d_6$) δ 123.84 (s), 128.42 (s), 132.44 (s), 149.12 (s) ppm. Slow evaporation from chloroform yielded tiny yellow crystals that were too small for single-crystal X-ray diffraction but whose IR spectrum and X-ray powder diffraction patterns (X-ray film methods, Cu radiation) were identical with those from crystals obtained from toluene. Stock solutions were prepared by dissolving **I** at 50°C in chloroform for 4 h in aluminum foil-covered flasks. Dilution of the stock solutions gave solutions of **I** in chloroform over a 0.25×10^{-5} – 35×10^{-5} M (0.031 – 4.3 mM) concentration range. Analytical-reagent chloroform (containing 0.75% ethanol as a stabilizer) was used as received.

N-Methyl-4-thiopyridone. Orange crystals were obtained from Professor P. Beak's laboratory, University of Illinois;³ m.p. 90–130°C; IR (Nujol), 3410 (broad), 1628, 1209, 1111, 1025, 819 cm^{-1} ; ^1H NMR (D_2O), δ 7.78–7.75 (d, 2H, $J = 6.8$ Hz), 7.54–7.51

(d, 2H, $J = 6.8$ Hz), 3.93 (s, 3H) ppm. Impurity peaks were observed in the NMR spectrum. The impurities did not interfere with the solvatochromic measurements performed to approximate the molar absorptivity of 4TP.

Oxidative degradation of 4-mercaptopyridine. Solutions of **I** in chloroform undergo light-catalyzed oxidation via formation of the 4,4'-pyridyldisulfide.⁴ The stability of **I** was examined by monitoring the 4TP absorbance intensity over time. The half-life of a solution of **I** exposed to ambient light was 11 h, whereas, no measureable decrease in the 4TP absorbance intensity occurred for solutions shielded from light. To prevent degradation, all solutions were prepared and shielded from light in vials and volumetric flasks covered with aluminum foil.

4-Hydroxypyridine-4-pyridone (II). Technical grade (90%) **II**, purchased from Aldrich, was recrystallized from THF-benzene (2:1) to yield a white flaky powder; m.p. 142–150°C; IR (Nujol), 3198, 3044, 2657, 1634, 1540, 1509, 1466, 1385, 1191, 834 cm^{-1} ; ^1H NMR (CDCl_3) δ 7.57–7.61 (d, 2H, $J = 8.01$), 6.44–6.48 (d, 2H, $J = 8.01$) ppm.

Solution aggregation calculations. The equilibrium concentrations of species in solution were calculated using equations (1)–(5). These equations were derived for the tautomerization and extended 4MP and 4TP self-association equilibria depicted in Scheme 1. The root, $X_{4\text{MP}}$, of the fourth-order polynomial in equation (1) was determined using the Newton-Raphson method.⁵ The aggregation curves for 4TP were formed by plotting $(X_s - X_{s,4\text{MP}})/(X_e - X_{s,4\text{MP}})$ vs $(X_e - X_{s,4\text{MP}})$, where the quantity $(X_s - X_{s,4\text{MP}})/(X_e - X_{s,4\text{MP}})$ is designated as the 4TP aggregation number. For the case where the 4MP aggregation is negligible, i.e. $K_{4\text{MP}} = 0$, the slope of the 4TP aggregation curve directly gives $K_{4\text{TP}}$.⁶ Oligomer distributions were calculated using the same equations applied to calculate the most probable molecular weight distributions for condensation polymerizations.⁷

$$\begin{aligned} & (K_1^2 K_{4\text{TP}}^2 K_{4\text{MP}}^2 X_s) X_{4\text{MP}}^4 - (2K_1^2 K_{4\text{TP}}^2 K_{4\text{MP}} X_s \\ & + 2K_{2\text{T}} K_{4\text{TP}} K_{4\text{MP}}^2 X_s + K_{\text{T}} K_{4\text{MP}}^2 + K_1^2 K_{4\text{TP}}^2) X_{4\text{MP}}^3 \\ & + (K_1^2 K_{4\text{TP}}^2 X_s + 4K_{\text{T}} K_{4\text{TP}} K_{4\text{MP}} X_s + K_{4\text{MP}}^2 X_s \\ & + 2K_{\text{T}} K_{4\text{MP}} + 2K_{\text{T}} K_{4\text{TP}}) X_{4\text{MP}}^2 \\ & - (2K_{\text{T}} K_{4\text{TP}} X_s + 2K_{4\text{MP}} X_s + K_{\text{T}} + 1) X_{4\text{MP}} + X_s = 0 \end{aligned} \quad (1)$$

$$X_e = \frac{K_{\text{T}} X_{4\text{MP}}}{(1 - K_{\text{T}} K_{4\text{TP}} X_{4\text{MP}})} + \frac{X_{4\text{MP}}}{(1 - K_{4\text{MP}} X_{4\text{MP}})} \quad (2)$$

Table 1. Crystal data, data collection and structure solution and refinement for 4TP

Crystal data:	
Formula	C ₅ H ₅ NS
Formula weight	111.16
Crystal color, habit	Yellow, hexagonal
Crystal dimensions (mm)	0.50 × 0.50 × 0.25
Space group	<i>P</i> 2 ₁ / <i>c</i>
<i>Z</i>	4
<i>d</i> _{calc} (g cm ⁻³)	1.44
<i>a</i> (Å)	7.183(5)
<i>b</i> (Å)	6.132(5)
<i>c</i> (Å)	11.618(7)
β (°)	90.51(5)
<i>V</i> (Å ³)	512(1)
<i>F</i> (000)	232
Data collection:	
Diffractometer	Enraf-Nonius CAD-4
Radiation	Mo K α (λ = 0.71069 Å), graphite-monochromated
μ (Mo K α) (cm ⁻¹)	4.6
<i>T</i> (°C)	-89(1)
Scan type	ω - 2 θ
2 θ _{max} (°)	60.0
<i>hkl</i> range	-10 ≤ <i>h</i> ≤ 10, -8 ≤ <i>k</i> ≤ 8, 0 ≤ <i>l</i> ≤ 16
Total reflections measured	2733
Unique reflections measured ^a	1623
Corrections	Lorentz polarization, absorption ^b (Transmission factors: 0.69–1.26), decay (-9.20% decline), secondary extinction (coefficient: 0.3130 × 10 ⁻⁶)
Structure solution and refinement:	
Structure solution	Direct methods ^c
Refinement	Full-matrix least-squares, ^d non-H atoms anisotropic, H atom on N1 refined as isotropic, other H atoms at idealized positions ^e and not refined
Unique observed reflections ^f	1154
Number of variable parameters	69
Residuals: <i>R</i> , ^g <i>wR</i> ^h	0.050, 0.072
Goodness of fit	1.91
Max. shift/error	0.00
Max. difference peak (e ⁻ Å ⁻³)	0.44
Min. difference peak (e ⁻ Å ⁻³)	-0.43

^a *R*_{int} = 0.087. Owing to the high value for *R*_{int}, symmetry equivalent pairs of reflections were examined. Discrepancies in intensity were observed for a number of reflections but there was no systematic pattern for this error. Intensities for equivalent reflections were averaged and their square roots calculated to give values for *F*_{observed}. These values were in good agreement with values for *F*_{calculated}.

^b DIFABS: N. Walker and D. Stuart, *Acta Crystallogr., Sect. A* **39**, 158–166 (1983).

^c MITHRIL: C. J. Gilmore, *J. Appl. Crystallogr.* **17**, 42–46 (1984). DIRDIF: P. T. Beurskens, W. P. Bosman, H. M. Doesburg, R. O. Gould, Th. E. M. Van Den Hark, P. A. J. Prick, J. H. Noordik, G. Beurskens, V. Parthasarathi, H. J. Bruins Slot and R. C. Haltwanger, *DIRDIF. Direct Methods for Difference Structures—An Automatic Procedure for Phase Extension and Refinement of Difference Structure Factor*, Tech. Rep. 1984/1. Crystallography Laboratory, Toernooiveld, Nijmegen (1984).

^d TEXSAN—TEXRAY Structure Analysis Package, Molecular Structure Corp. (1985).

^e *d*_{C-H} = 0.95 Å, *B* = 1.2 (*B*_{equivalent} of bonded atom).

^f *I* > 3σ(*I*).

^g *R* = Σ ||*F*_o|| - ||*F*_c|| / Σ ||*F*_o||.

^h *wR* = [(Σ *w*(||*F*_o|| - ||*F*_c||)² / Σ *wF*_o²]^{1/2}; *w* = 4*F*_o² / σ²(*F*_o²).

Table 2. Fractional atomic coordinates for 4TP

Atom	<i>x/a</i>	<i>y/b</i>	<i>z/c</i>
S1	0.75381(7)	-0.16334(9)	0.95989(4)
N1	0.7475(3)	0.3110(3)	0.6652(2)
C1	0.8192(3)	0.1105(4)	0.6498(2)
C2	0.8229(3)	-0.0376(3)	0.7387(2)
C3	0.7515(2)	0.0170(3)	0.8484(2)
C4	0.6774(3)	0.2306(4)	0.8587(2)
C5	0.6777(3)	0.3716(4)	0.7675(2)
H1	0.8669	0.0700	0.5769
H2	0.8761	-0.1768	0.7259
H4	0.6272	0.2755	0.9303
H5	0.6274	0.5139	0.7771
H1N	0.747(4)	0.393(7)	0.611(4)

$$X_{s,4MP} = \frac{X_{4MP}}{(1 - K_{4MP}X_{4MP})^2} \quad (3)$$

$$X_{s,4TP} = X_s - X_{s,4MP} \quad (4)$$

$$X_{4TP} = K_T(X_{4MP}) \quad (5)$$

where

X_{4MP} = mole fraction concentration of 4MP monomer;

X_{4TP} = mole fraction concentration of 4TP monomer;

X_s = stoichiometric concentration of 4-mercaptopyridine-4-thiopyridone in all forms in solution;

$X_{s,4MP}$ = stoichiometric concentration of 4MP

$$= \sum_{n=1}^{\infty} nX_{(4MP)_n};$$

$X_{s,4TP}$ = stoichiometric concentration of 4TP

$$= \sum_{n=1}^{\infty} nX_{(4TP)_n};$$

X_e = effective solute concentration

$$= \sum_{n=1}^{\infty} [X_{(4MP)_n} + X_{(4TP)_n}];$$

K_T = tautomerization constant;

K_{4TP} = 4TP self-association constant;

K_{4MP} = 4MP self-association constant.

Crystal structure determination. Crystal data, data collection and structure solution details for **I** are given in Table 1. Fractional atomic coordinates are given in Table 2.

Cambridge Structural Database (CSD) searches. To test whether the C—S bond length of **I** was consistent with 4TP or 4MP, substructure searches on thiol

(C—S—H) and thione [C—(C=S)—C] fragments were performed on the CSD (Version 4.1, 82129 entries)⁸ using the *CONNser test. Structures containing both thiol and thione fragments were excluded. Only those structures with $R \leq 0.075$ and containing only main group elements were accepted. C—S bond lengths were computed using GSTAT89 (CSD software) and bond lengths differing by more than 4σ from the mean C—S distance were ignored. The final data set gave 14 unique thiol C—S distances and 23 unique thione C=S distances.

RESULTS

Crystal structure results

Intramolecular structure

In order to identify which tautomeric form exists in the solid state, the intramolecular bond lengths of **I** were compared with the corresponding bond lengths from the neutron diffraction crystal structure of 2-thiopyridone⁹ and the C=S bond length was compared with the mean C—S and C=S bond lengths retrieved from a search of thiol and thione crystal structures from the CSD. X-ray data from **I** give a C=S bond length of 1.703(2) Å, which is close to the value of 1.698(2) Å for 2-thiopyridone. The C—C bond lengths of **I** range from 1.368(3) to 1.419(3) Å, and both C—N bond lengths are 1.346(3) Å. These distances are also consistent with the corresponding single and double bond lengths observed in the neutron structure for 2-thiopyridone. The distribution plot of thiol bond lengths and thione bond lengths from the CSD is shown in Figure 1. Mean C—S bond lengths of 1.81(2) and 1.66(4) Å are calculated for the thiols and thiones, respectively. The C—S bond length of **I** matches the

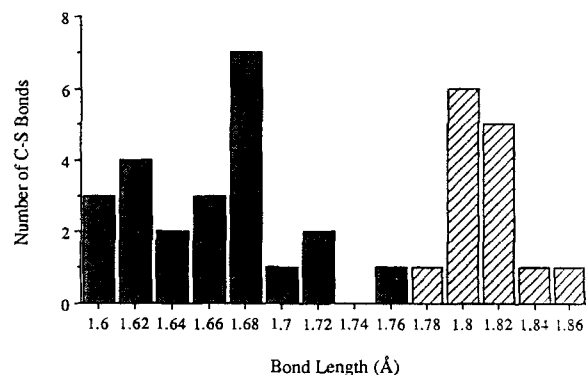
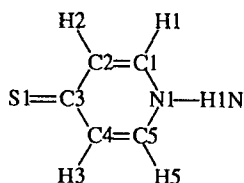


Figure 1. Distribution of thione (shaded) and thiol (striped) bond lengths obtained from the Cambridge Structural Database

Table 3. Selected intramolecular bond lengths and angles and hydrogen-bond geometry for 4TP



Selected intramolecular bond lengths and angles:

S1—C3 (Å)	1.703(2)	S1—C3—C2 (°)	121.9(2)
N1—H1N (Å)	0.81(4)	S1—C3—C4 (°)	122.4(2)
N1—C1 (Å)	1.346(3) ^a	N1—C1—C2 (°)	120.6(2)
N1—C5 (Å)	1.346(3) ^a	N1—C5—C4 (°)	120.8(2)
C1—C2 (Å)	1.375(3)	C1—N1—H1N (°)	117(3)
C2—C3 (Å)	1.419(3) ^a	C1—N1—C5 (°)	121.0(2)
C3—C4 (Å)	1.419(3) ^a	C1—C2—C3 (°)	120.9(2)
C4—C5 (Å)	1.368(3)	C2—C3—C4 (°)	115.6(2)
		C3—C4—C5 (°)	121.0(2)
		C5—N1—H1N (°)	122(3)

Intermolecular hydrogen-bond geometry:

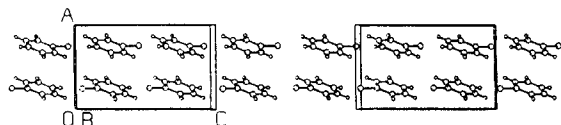
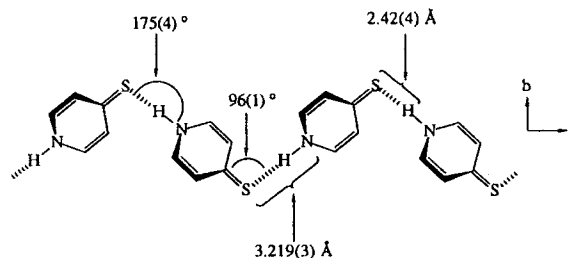
N1...S1	3.219(3)	N1—H1N...S1 (°)	175(4)
H1N...S1	2.42(4)	C3—S1...H1N (°)	96(1)

^a The numbers in these two pairs are coincidentally identical.^b Molecules related as x, y, z and $x, \frac{1}{2} - y, -\frac{1}{2} + z$

mean C=S bond length retrieved from the CSD much more closely than the mean C—S bond length. In addition, the acidic hydrogen of **I** was located close to nitrogen in an electron density difference map and refined to give an N—H distance of 0.81(4) Å. The molecular structure of **I**, therefore, is consistent with an assignment of 4TP rather than 4MP. Selected intramolecular bond lengths and angles for 4TP are given in Table 3. Least-squares planes analyses indicate that the aromatic ring is planar and that the S atom deviates only 0.002 Å from the mean plane of the ring.

Intermolecular structure

N—H...S hydrogen bonds are the most salient feature of the molecular packing giving rise to hydrogen-bonded chains of *c*-glide related molecules (Figure 2). The chains are related to one another by inversion centers. The N...S distance in the hydrogen bond is

Figure 2. Stereo view of the molecular packing of 4TP. Hydrogen-bonded chains extend along the *c* axis of the unit cellFigure 3. Hydrogen-bonded chain of *c*-glide related molecules in the crystal structure of 4TP projected onto (100). The vector passing through the S—N axis of 4TP is tilted out of the (100) plane by 1° and the ring is rotated 25° from (100) about the S—N axis

3.219(3) Å (van der Waals sum = 3.35 Å)¹⁰ and the N—H...S angle is 175(4)°. The C—S...H angle is 96(1)° so that each molecule is aligned with its long axis at nearly right-angles to its nearest neighbors forming a kinked chain (Figure 3). The 96° C—S...H angle is reasonable as 90° hydrogen bonds to sulfur have been observed in gas-phase hydrogen-bond complexes.¹¹ Selected intermolecular hydrogen-bond lengths and angles for 4TP are given in Table 3.

Solution association of 4TP

As depicted in Scheme 1, both 4-mercaptopyridine (4MP) and 4-thiopyridone (4TP) can self-associate in solution to form hydrogen-bonded oligomers, (4MP)_n and (4TP)_n. These two self-association equilibria are linked by the tautomerization constant, *K*_T. The determination of *K*_T from the equilibrium monomer concentrations of each tautomer is complicated by the oligomerization equilibria, since the UV–visible spectra of the oligomer and monomer overlap, as shown in Figure 4. For example, as the 4TP aggregation increases from 1.2% to 55%, the 4TP λ_{max} shifts only slightly from 356 to 354 nm. The close similarity of the monomer and oligomer spectra implies that the hydrogen bonding of 4TP to solvent is similar to that within an oligomer and that the electronic perturbation experienced by 4TP within an oligomer closely matches that of solvated 4TP monomer. Therefore, the total concentration of 4TP was measured using either the absorbance at 354 or 356 nm. No quantifiable absorbance maximum was observed for 4MP; therefore, the 4MP concentration was measured from the difference between the concentration of **I** and the measured 4TP concentration.

A prerequisite for determining the 4TP concentration is a knowledge of its molar absorptivity (ε_{4TP}) at λ_{max}. Unfortunately, this value (in chloroform) is not known and cannot be directly determined spectroscopically because of the tautomerization. Therefore, ε_{4TP} was

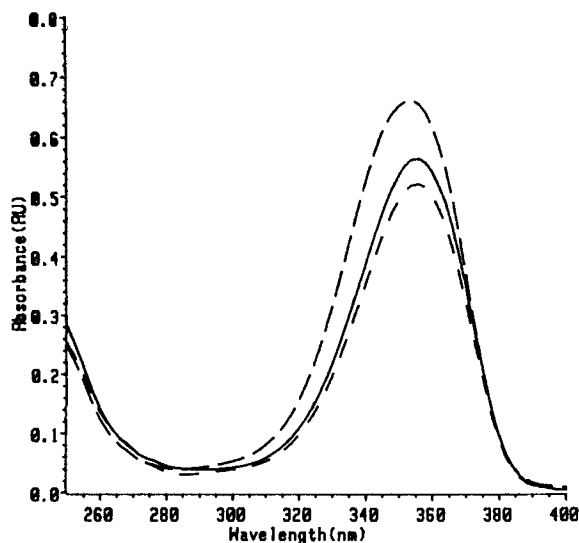


Figure 4. UV-visible solution spectra of **I** in chloroform over a 100-fold concentration range. (---) 35×10^{-5} mf, 0.01 cm cell path; (—) 3.5×10^{-5} mf, 0.1 cm cell path; (- - -) 0.35×10^{-5} mf, 1 cm cell path

estimated from a solvatochromic comparison of it with its methylated analog, *N*-methyl-4-thiopyridone. *N*-Methyl-4-thiopyridone does not tautomerize and consequently its molar absorptivity can be readily determined by measuring the absorbance of standard solutions. The value of ϵ_{4TP} in ethanol is known and can be easily measured, since 4TP is highly favored in ethanol.¹² The value of ϵ_{4TP} in chloroform was approximated by comparing its UV-visible spectra in ethanol and in chloroform with those of *N*-methyl-4-thiopyridone. As seen in Figure 5, both *N*-methyl-4-thiopyridone and 4TP exhibit nearly the same solvatochromic effect. The molar absorptivity of *N*-methyl-4-thiopyridone was 14.2% less in chloroform than in ethanol. The value of ϵ_{4TP} in chloroform was determined by applying the same fractional decrease observed for the molar absorptivity of *N*-methyl-4-thiopyridone to the ϵ_{4TP} in ethanol. The resulting ϵ_{4TP} in chloroform at λ_{max} was $19,140 \text{ l mol}^{-1} \text{ cm}^{-1}$.

The 4TP concentration measured at either the 354 or 356 nm λ_{max} is a sum total of the 4TP monomer concentration and the stoichiometric concentration of 4TP in oligomer. As the concentration decreases, aggregation also decreases. Consequently, the measured 4TP concentration approaches that of 4TP monomer and the ratio of the 4TP/4MP concentrations approaches that of the monomer concentration ratio which is K_T . In Table 4, the 4TP/4MP concentration ratios are listed over a 100-fold concentration range. The tautomeric ratio decreases with decreasing concentration and reaches a constant value of 1.8 below 1×10^{-5} mf

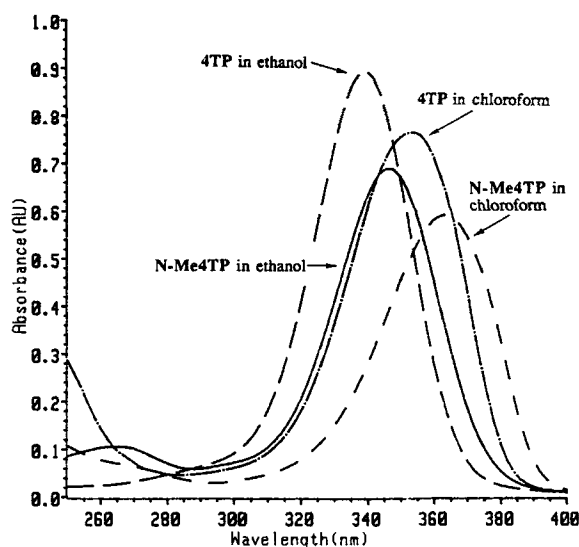


Figure 5. UV-visible spectra of 4 mm solutions of 4TP and *N*-methyl-4-thiopyridone in ethanol and chloroform. (---) 4TP in ethanol; (- - -) 4TP in chloroform; (—) *N*-Me4TP in ethanol; (- - -) *N*-Me4TP in chloroform. The shifts in λ_{max} for 4TP and *N*-methyl-4-thiopyridone are 14 and 18 nm, respectively

(0.12 mM). The value of K_T , therefore, was found to be 1.8 ± 0.2 .

The non-constant tautomeric ratio and, in particular, the increasing tautomeric ratio with increasing concentration, exhibited in Table 4, are indicative of 4TP oligomerization. Further evidence of 4TP aggregation is observed from the increase in 4TP aggregation number with increase in concentration, as demonstrated by the 4TP aggregation curve in Figure 6. The increase in 4TP concentration is, of course, dependent on K_{4TP} , but also on K_T and K_{4MP} since these equilibria dictate how much 4TP is available to oligomerize. Calculated 4TP concentrations over a range of K_T , K_{4MP} and K_{4TP} values

Table 4. Tautomeric ratio of **I** over a 100-fold concentration range

Concentration (mole fraction $\times 10^{-5}$)	Tautomeric ratio [4TP]/[4MP]
35	3.9
20	2.9
10	2.5
5.0	2.4
2.0	2.1
1.0	1.8
0.5	1.8
0.25	1.8

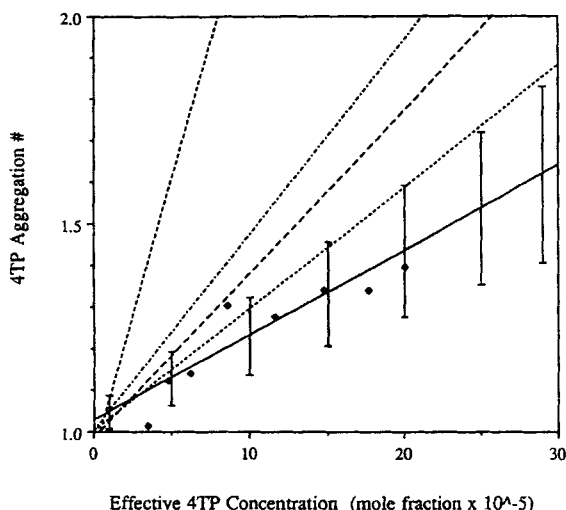


Figure 6. Comparison of calculated versus measured aggregation curves. (—) Measured 4TP aggregation curve from vapor pressure osmometry. Calculated curves: (---) $K_T = 1.8$, $K_{4TP} = 8000 \text{ mf}^{-1}$, $K_{4MP} = 8000 \text{ mf}^{-1}$; (----) $K_T = 1.8$, $K_{4TP} = 4000 \text{ mf}^{-1}$, $K_{4MP} = 2000 \text{ mf}^{-1}$; (---) $K_T = 1.8$, $K_{4TP} = 2600 \text{ mf}^{-1}$, $K_{4MP} = 2600 \text{ mf}^{-1}$; (···) $K_T = 1.8$, $K_{4TP} = 2600 \text{ mf}^{-1}$, $K_{4MP} = 1000 \text{ mf}^{-1}$

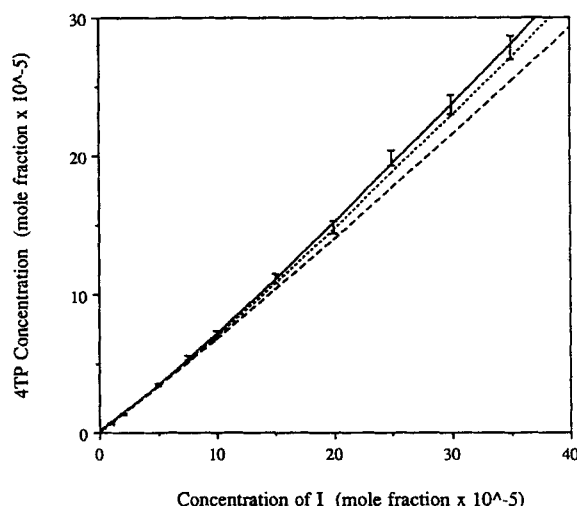


Figure 7. Comparison of calculated 4TP concentration curves to the measured increase in 4TP concentration over a 100-fold concentration range. Experimental data is shown with error bars. Calculated curves: (---) $K_T = 1.8$, $K_{4TP} = 2600 \text{ mf}^{-1}$, $K_{4MP} = 2600 \text{ mf}^{-1}$; (···) $K_T = 1.8$, $K_{4TP} = 2600 \text{ mf}^{-1}$, $K_{4MP} = 1000 \text{ mf}^{-1}$; (—) $K_T = 1.8$, $K_{4TP} = 2600 \text{ mf}^{-1}$, $K_{4MP} = 0 \text{ mf}^{-1}$

were compared with the increase in 4TP concentration observed experimentally. The examination consisted of systematically incrementing and decrementing K_T , K_{4MP} and K_{4TP} in steps of 0.2, 200 and 500, respectively. Different sets of equilibrium constants can be found to fit the data. For example, the following $[K_T, K_{4TP}, K_{4MP}]$ ordered triads of equilibrium constants all satisfy the UV-visible data: $[1.8, 800, 8000]$, $[1.8, 4000, 2000]$ and $[1.8, 2600, 0]$. However, as shown in Figure 6 they do not all agree with vapor pressure osmometry results. In addition, agreement between the measured and calculated data and between the UV-visible and vapor pressure osmometry data is only observed when K_{4MP} is much smaller than K_{4TP} (Figures 6 and 7). The best overall agreement between the calculated and observed 4TP concentrations over a 100-fold concentration range is illustrated in Figure 7. The results indicate that the 4-mercaptopyridine-4-thiopyridone system can be best represented solely by the tautomerization and 4TP oligomerization equilibria with $K_T = 1.8$ and $K_{4TP} = 2600 \text{ mf}^{-1}$. This value for K_{4TP} , $2600 \pm 400 \text{ mf}^{-1}$, determined from UV-visible absorbance data, matches within experimental certainty to that obtained from the vapor pressure osmometry measurements, $2040 \pm 300 \text{ mf}^{-1}$. A further cross-check of these results can be made by monitoring the relative increase in the 4TP absorbance with increase in concentration. This analysis does not require the use of the estimated ϵ_{4TP} . The best values for the equilibrium con-

stants determined from iterative calculations of the 4TP concentration data also fit the increase in relative 4TP absorbance over the experimental concentration range (Figure 8). The distribution of 4TP oligomers at 25°C near saturation ($56 \times 10^{-5} \text{ mf}$; 7 mM) is calculated for the 4TP self-association constant (K_{4TP}) of 2600 mf^{-1} in Figure 9.

It is implied from the linearity of the vapor pressure osmometry data that the hydrogen-bond energy is constant, within the sensitivity of the measurement, along each step of the oligomer growth. The near coincidence of the UV-visible spectra of the solvated 4TP monomer and the 4TP oligomer also suggests that the hydrogen-bond stabilization experienced by a 4TP monomer within an oligomer chain is similar to that of a chloroform-solvated monomer. Throughout the analysis of the self-association of 4TP, it has been assumed that the formation constants, as defined in Scheme I, along each step of the hydrogen-bonded oligomer chain growth are equal. Theoretical discussions of the hydrogen-bond cooperativity effect¹² and entropic arguments,¹³ however, have indicated that the dimerization constant should be less than the oligomerization constant. These theoretical predictions have been substantiated experimentally for the self-association of *N*-methylacetamide in certain solvents,¹⁴ although no significant difference was observed between the dimerization and oligomerization constants for *N*-methylacetamide in chloroform.¹⁵ It is implied from

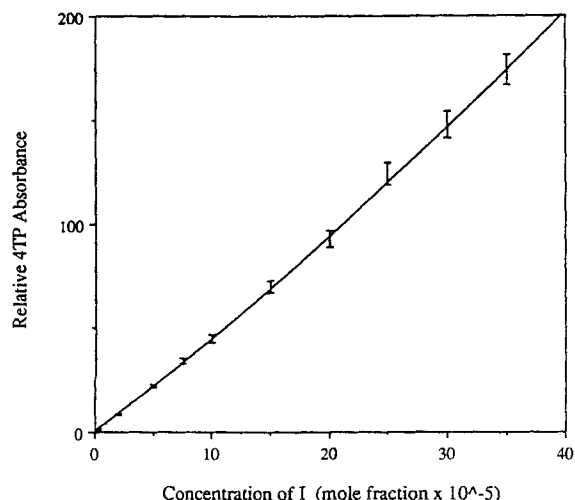


Figure 8. Agreement between the calculated relative increase in the 4TP absorbance for $K_T = 1.8$, $K_{4TP} = 2600 \text{ mf}^{-1}$ and $K_{4MP} = 0 \text{ mf}^{-1}$ to the measured relative increase in the 4TP absorbance at λ_{max} with concentration. Experimental data is shown with error bars

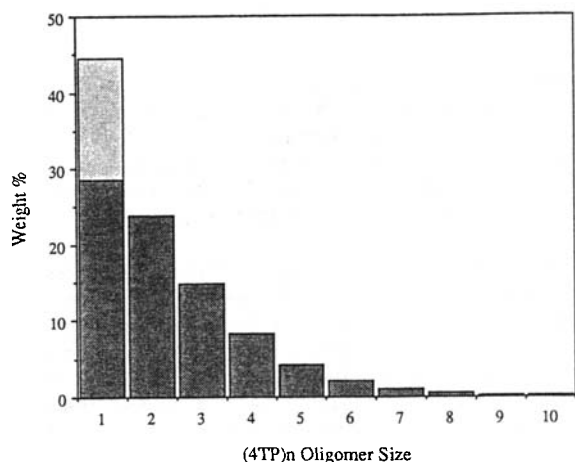


Figure 9. Distribution of **I**, by weight, among various $(4TP)_n$ oligomeric species at $56 \times 10^{-5} \text{ mf}$ (7 mM) in chloroform at 25°C . The monomer segment is divided to show the relative amounts of 4MP monomer (light region) and 4TP monomer (dark region)

the linearity of the VPO data that the hydrogen-bond energy is constant, within the sensitivity of the measurement, along each step of the oligomer growth. The near coincidence of the UV-VIS spectra of the solvated 4TP monomer and the 4TP oligomer also suggests that the hydrogen-bond stabilization experienced by a 4TP monomer within an oligomer chain is similar to that of

a chloroform-solvated monomer. To check the comparability of the dimerization and oligomerization constants for 4TP in chloroform, the 4TP dimerization constant was estimated using an extrapolation procedure on the 4TP aggregation data.^{6a} The resulting dimerization constant for 4TP in chloroform ($2260 \pm 170 \text{ mf}^{-1}$) is not significantly different from the oligomerization constant ($2600 \pm 400 \text{ mf}^{-1}$). Therefore, a single step-wise formation constant was applied to the 4TP aggregation; no additional parameter was needed to account for the dimerization.

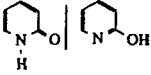
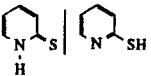
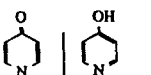
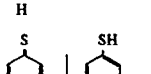
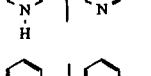
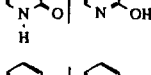
DISCUSSION

Previous studies have shown that related hydroxypyridine-pyridone and mercaptopyridine-thiopyridone compounds have high association constants in solution (Table 5). For example, K_{assoc} of 4-pyridone in chloroform at room temperature is 30000 mf^{-1} , whereas K_{assoc} of benzoic acid dimers¹⁶ in chloroform is 5000 mf^{-1} and the intramolecular K_{assoc} of covalently tethered lactams¹⁷ in chloroform is 300 mf^{-1} . The self-association for either the hydroxypyridine-pyridones or the mercaptopyridine-thiopyridones tends to be greater in non-polar solvents, and the tautomerization constants tends to be larger in polar solvents.¹⁸ The tautomerization and self-association constants of the hydroxypyridine-pyridone compounds are generally higher than those of their corresponding sulfur analogs. Aggregate structures of the *para*-substituted compounds are oligomers rather than entropically more favorable dimers. These extended hydrogen-bonded aggregates form even though there is no topological stabilization, as for crown ether complexes, and only monodentate hydrogen bonds exist between neighboring molecules.

The solution behavior of **I** is similar to that of its oxygen analog, **II**, although the predominance of 4TP and its associated aggregates over 4MP is not as great as that of 4P over 4HP for **II** in chloroform. For both **I** and **II**, the predominant solution tautomer is also observed in the solid state.¹⁹

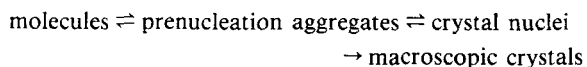
In principle, a minor solution aggregate form could nucleate crystal growth, and thus be found in the solid state. For **I** and **II**, if a small amount of $(4MP)_n$ or $(4HP)_n$ nucleated crystal growth, then the equilibria in Scheme 1 would be displaced toward the minor tautomer as crystallization removed it from solution. However, for **I** and **II**, hydrogen-bonded aggregates of the dominant tautomeric form in solution are found in the solid state. Presumably, it is precisely these hydrogen-bonded solution aggregates which nucleated and sustained crystal growth. In studies of asymmetric and symmetric dipyrindones, Ducharme and Wuest²⁰ likewise noted that the dominant hydrogen-bonded aggregates observed in chloroform solution were also observed in the solid state.

Table 5. Self-association and tautomerization constants of related hydroxypyridines/pyridones and mercaptopyridines/thiopyridones

Compound	Solvent	K_T	$K_{\text{assoc}; \text{N}-\text{H}}$	$K_{\text{assoc}; \text{N}^{\text{a}}}$	Temperature ($^{\circ}\text{C}$) ^b	Reference
	Chloroform	> 5	25,000	NR	27	2
	Chloroform	2.6	2700	ND	RT	21
	Chloroform	> 5	30,000	NR	RT	2, 22
	Chloroform	1.8	2600	0	25	This work
	Cyclohexane	1.6	56×10^5	ND	RT	21
	Cyclohexane	0.09	9.4×10^5	ND	RT	21

^a ND = no aggregate detected; NR = no reference was made to this value.^b RT = room temperature.

This one to one correspondence between solution and solid-state aggregate structures suggests that solution aggregates form prior to crystal nucleation. They may act as pre-nucleation aggregates, whereby crystal nucleation proceeds predominantly by association of these oligomers:



One implication of this proposed mechanism is that crystal growth or binding of small molecules to surfaces, at least in cases where intermolecular hydrogen bonding occurs, might profitably be modeled as a process of deposition of oligomers rather than as deposition of monomers to crystal surfaces.

These studies support our contention that solid-state structures give useful information about molecular recognition properties of molecules in solution, especially in those cases where solution equilibria are more complicated than simple dimerization and where the associated species are not easily characterized in solution.

ACKNOWLEDGEMENTS

We are particularly grateful to Professor Peter Beak, Department of Chemistry, University of Illinois, for his

many helpful comments about this work and for supplying samples of *N*-methyl-4-thiopyridone. We are also grateful to Professor Doyle Britton, Department of Chemistry, University of Minnesota, for providing crystallographic assistance, to Professor Jim Loehlin, Department of Chemistry, Wellesley College, for helpful discussions, and to NSF (CHE-8600383) and the Office of Naval Research for financial support.

REFERENCES

1. M. C. Etter, *J. Phys. Chem.* **95**, 4601–4610 (1991).
2. P. Beak, J. B. Covington, S. G. Smith, J. M. White and J. M. Zeigler, *J. Org. Chem.* **45**, 1354–1362 (1980).
3. P. Beak, F. S. Fry, Jr, J. Lee and F. Steele, *J. Am. Chem. Soc.* **98**, 171–179 (1976).
4. S. Stoyanov, I. Petkov, L. Antonov and T. Stoyanova, *Can. J. Chem.* **68**, 1482–1489 (1990).
5. *Hewlett-Packard HP-11c Owner's Handbook and Problem Solving Guide*, pp. 154–158. Hewlett-Packard, Avondale, PA (1985).
6. (a) M. Davies and D. K. Thomas, *J. Phys. Chem.* **60**, 763–766 (1956); (b) E. E. Schier, *J. Chem. Educ.* **45**, 176–180 (1968).
7. P. C. Hiemenz, *Polymer Chemistry*, pp. 292–299. Marcel Dekker, New York (1984).
8. F. H. Allen, S. A. Bellard, M. D. Brice, B. A. Cartwright, A. Doubleday, H. Higgs, T. Hummelink, B. G. Hummelink-Peters, O. Kennard, W. D. S. Motherwell,

- J. R. Rodgers and D. G. Watson, *Acta Crystallogr., Sect. B* **35**, 2331–2339 (1979).
9. U. Ohms, H. Guth, A. Kutoglu and C. Scheringer, *Acta Crystallogr., Sect. B* **38**, 831–834 (1982).
10. A. Bondi, *J. Phys. Chem.* **68**, 441–445 (1964).
11. A. C. Legon and D. J. Millen, *Acc. Chem. Res.* **20**, 39–46 (1987).
12. J. E. Del Bene, *J. Am. Chem. Soc.* **100**, 1387–1394 (1978).
13. L. Sarolea-Mathot, *Trans. Faraday Soc.* **49**, 8–20 (1953).
14. (a) L. L. Graham and C. Y. Chang, *J. Phys. Chem.* **75**, 776–783 (1971); (b) M. Davies and D. K. Thomas, *J. Phys. Chem.* **60**, 767–770 (1956); (c) L. L. Graham and C. Y. Chang, *J. Phys. Chem.* **75**, 784–788 (1971).
15. L. L. LaPlanche, H. B. Thompson and M. T. Rogers, *J. Phys. Chem.* **69**, 1482–1488 (1965).
16. Y. I'Haya, and T. Shibuya, *Bull. Chem. Soc. Jpn.* **38**, 1144–1147 (1965).
17. J. Rebek, Jr, K.-S. Jeong and T. Tjivikua, *J. Am. Chem. Soc.* **112**, 3215–3217 (1990).
18. P. Beak, *Acc. Chem. Res.* **10**, 186–192 (1977).
19. R. A. Jones and A. R. Katritzky, in *Physical Methods in Heterocyclic Chemistry*, edited by A. R. Katritzky, Vol. II, p. 260. Academic Press, New York, London (1963).
20. Y. Ducharme and J. D. Wuest, *J. Org. Chem.* **53**, 5789–5791 (1988).
21. P. Beak, J. B. Covington and S. G. Smith, *J. Am. Chem. Soc.* **98**, 8284–8286 (1976).
22. P. Beak, J. B. Covington and J. M. Zeigler, *J. Org. Chem.* **43**, 177–178 (1978).